Article

# Structures, Electronic States, Photoluminescence, and Carrier Transport Properties of 1,1-Disubstituted 2,3,4,5-Tetraphenylsiloles

Gui Yu, Shiwei Yin, Yunqi Liu, Jiangshan Chen, Xinjun Xu, Xiaobo Sun, Dongge Ma, Xiaowei Zhan, Qian Peng, Zhigang Shuai, Benzhong Tang, Daoben Zhu, Weihai Fang, and Yi Luo

*J. Am. Chem. Soc.*, **2005**, 127 (17), 6335-6346• DOI: 10.1021/ja044628b • Publication Date (Web): 12 April 2005



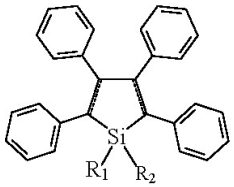


DMTPS: $R_1$=$R_2$=$CH_3$
MPPS: $R_1$=$CH_3$; $R_2$=Ph
HPS: $R_1$=$R_2$=Ph

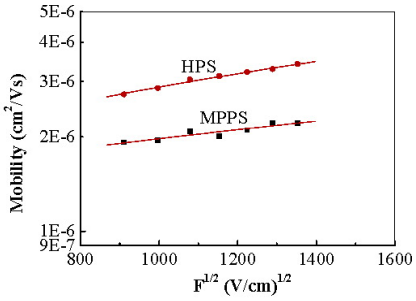


## More About This Article

Additional resources and features associated with this article are available within the HTML version:

- Supporting Information
- Links to the 45 articles that cite this article, as of the time of this article download
- Access to high resolution figures
- Links to articles and content related to this article
- Copyright permission to reproduce figures and/or text from this article

View the Full Text HTML

J|A|C|S
ARTICLES
Published on Web 04/12/2005

# Structures, Electronic States, Photoluminescence, and Carrier Transport Properties of 1,1-Disubstituted 2,3,4,5-Tetraphenylsiloles

Gui Yu,[†] Shiwei Yin,[†] Yunqi Liu,*[,†] Jiangshan Chen,[‡] Xinjun Xu,[†] Xiaobo Sun,[†] Dongge Ma,[‡] Xiaowei Zhan,[†] Qian Peng,[†] Zhigang Shuai,*[,†] Benzhong Tang,[§] Daoben Zhu,*[,†] Weihai Fang,[⊥] and Yi Luo[||]

*Contribution from the Organic Solids Laboratory, Institute of Chemistry, Chinese Academy of Sciences, Beijing 100080, P.R. China, Key State Laboratory of Polymer Physics and Chemistry, Changchun Institute of Applied Chemistry, Chinese Academy of Sciences, Changchun 130022, P.R. China, Department of Chemistry, Hong Kong University of Science & Technology, Clear Water Bay, Kowloon, Hong Kong, P.R. China, Department of Chemistry, Beijing Normal University, Beijing 100875, P.R. China, and Theoretical Chemistry, Royal Institute of Technology, AlbaNova, Stockholm S-106 91, Sweden*

Received September 3, 2004; E-mail: liuyq@mail.iccas.ac.cn

***Abstract:*** The excellent electroluminescent (EL) properties of 1,1-disubstituted 2,3,4,5-tetraphenylsiloles, 1-methyl-1,2,3,4,5-pentaphenylsilole (MPPS), and 1,1,2,3,4,5-hexaphenylsilole (HPS) have been found. Despite some studies devoted to these materials, very little is known about the real origin of their unique EL properties. Therefore, we investigated the structures, photoluminescence (PL), and charge carrier transport properties of 1,1-disubstituted 2,3,4,5-tetraphenylsiloles as well as the effect of substituents on these characteristics. The single crystals of the three siloles involving 1,1-dimethyl-2,3,4,5-tetraphenylsilole (DMTPS), MPPS, and HPS were grown and their crystal structures were determined by X-ray diffraction. Three siloles have nonplanar molecular structures. The substituents at 1,1-positions enhance the steric hindrance and have predominant influence on the twisted degree of phenyl groups at ring carbons. This nonplanar structure reduces the intermolecular interaction and the likelihood of excimer formation, and increases PL efficiency in the solid state. The silole films show high fluorescence quantum yields (75−85%), whereas their dilute solutions exhibit a faint emission. The electronic structures of the three siloles were investigated using quantum chemical calculations. The highest occupied molecular orbitals (HOMOs) and the lowest unoccupied molecular orbitals (LUMOs) are mainly localized on the silole ring and two phenyl groups at 2,5-positions in all cases, while the LUMOs have a significant orbital density at two exocyclic Si−C bonds. The extremely theoretical studies of luminescent properties were carried out. We calculated the nonradiative decay rate of the first excited state as well as the radiative one. It is found that the faint emission of DMTPS in solutions mainly results from the huge nonradiative decay rate. In solid states, molecular packing can remarkably restrict the intramolecular rotation of the peripheral side phenyl ring, which has a large contribution to the nonradiative transition process. This explains why the 1,1-disubstituted 2,3,4,5-tetraphenylsiloles in the thin films exhibit high fluorescence quantum yields. The charge carrier mobilities of the MPPS and HPS films were measured using a transient EL technique. We obtained a mobility of $2.1 \times 10^{-6}$ cm$^2$/V·s in the MPPS film at an electric field of $1.2 \times 10^6$ V/cm. This mobility is comparable to that of $Alq_3$, which is one of the most extensively used electron transport materials in organic light-emitting diodes (LEDs), at the same electric field. The electron mobility of the HPS film is about ∼1.5 times higher than that of the MPPS film. To the best of our knowledge, this kind of material is one of the most excellent emissive materials that possess both high charge carrier mobility and high PL efficiency in the solid states simultaneously. The excellent EL performances of MPPS and HPS are presumably ascribed to these characteristics.

## Introduction

Since the reports by Tang[1] and Burroughes,[2] organic and polymer light-emitting diodes (LEDs), which are generally composed of thin multilayers of hole-transporting (HT), emissive, and electron-transporting (ET) materials sandwiched between two electrodes, have attracted much attention because of their possible application as new display devices.[3,4] Since then, many organic and polymer materials have been shown to be useful electroluminescent (EL) materials.[5,6] One of the current subjects to emerge in this field is the development of efficient EL materials, which can offer excellent charge carrier transport

[†] Institute of Chemistry, Chinese Academy of Sciences.
[‡] Changchun Institute of Applied Chemistry, Chinese Academy of Sciences.
[§] The Hong Kong University of Science and Technology.
[⊥] Beijing Normal University.
[||] Royal Institute of Technology.

10.1021/ja044628b CCC: $30.25 

properties and high photoluminescence (PL) quantum yields ($\Phi_{PL}$) in solid states. The representative ET materials used thus far are rather restricted to a few types of compounds, such as C═N double-bond-containing heteroaryls and their metal complexes,[7] metal−quinolinol complexes,[8] cyano-substituted poly(*p*-phenylenevinylene)s,[9] and boron-substituted oligothiophenes.[10] However, few organic compounds exhibit both high electron mobility and high $\Phi_{PL}$ in the amorphous solid state. Tris(8-hydroxyquinolinolato)aluminum ($Alq_3$) is one of the most widely used ET materials with high mobility in organic LEDs. However, $Alq_3$ exhibits a very low $\Phi_{PL}$.[11] Simultaneously, the mobility of $Alq_3$ is lower than that of HT materials, such as *N*,*N*′-diphenyl-*N*,*N*′-bis(1-naphenyl)-1,1′-biphenyl-4,4′-diamine (NPB) and *N*,*N*′-diphenyl-*N*,*N*′-di(3-methylphenyl)-1,1′-biphenyl-4,4′-diamine (TPD).[12] In an organic LED using NPB or TPD as the HT layer and $Alq_3$ as the ET layer, the transport of holes and electrons will be unbalanced. Due to this fact, it is desirable to design molecules with both high charge carrier mobility and high $\Phi_{PL}$.

Most of luminescent materials are highly emissive in their dilute solutions but become weakly luminescent when fabricated into thin films. In the solid state, the molecules aggregate to form less emissive species such as excimers, leading to a reduction in the luminescence efficiency. To realize high $\Phi_{PL}$ in the solid films, doping of a highly fluorescent or phosphorescent molecule (guest) into the emitting layer (host) has been accepted as the most effective approach. Energy transfers from the host to the guest molecules and/or direct carrier combination on the guest molecules contributes to an efficient emission from the guest. Although doping offers a high $\Phi_{PL}$ and other advantages such as an improvement of external EL quantum efficiency ($\eta_{EL}$), it complicates the fabrication process, requires careful selection of the guest and host molecules to maximize energy transfer, and increases the cost of production. Thus, it would be ideal if one can achieve very high $\Phi_{PL}$ in an undoped solid film.

Aggregation quenching has been the thorniest problem in the development of organic LEDs because in LEDs organic materials are predominately used as thin solid films, in which aggregation is inherently accompanied with the film formation.[13] Mitigation of the aggregation quenching has been a goal of research. An intriguing phenomenon of aggregation-induced emission (AIE) in siloles has been observed.[14] 2,3,4,5-Tetraphenylsilole derivatives are faintly emissive in ethanol or chloroform solutions, but their aggregates or solid states are strongly luminescent: the $\Phi_{PL}$ of the silole aggregates can differ from that of their molecularly dissolved species by 2 orders of magnitude. A serious difficulty with regard to understanding the intriguing phenomenon is that there is insufficient knowledge about the optical and electronic properties of the materials in solid states (i.e., single crystals and thin film) and solutions. These properties are strongly coupled to molecular structures and bulk molecular packing characteristics.[15] However, there are few investigations on the molecular structure, the molecular packing, the morphological properties in the thin films, and the corresponding optical/electronic properties in organic/polymeric materials.[16] Metal tris-complexes with asymmetric ligands can have either a meridional (*mer*) or a facial (*fac*) configuration. The two isomers give rise to different stabilities, different electronic behaviors, different photophysical characteristics, and different electrochemical properties.[17,18] Moreover, in the case of *mer*-$Alq_3$, the solvated and unsolvated molecular structures are different, which are responsible for the remarkable varieties


(1) Tang, C. W.; VanSlyke, S. A. *Appl. Phys. Lett.* **1987**, *51*, 913−915.
(2) Burroughes, J. H.; Bradly, D. D. C.; Broun, A. R.; Marks, R. N.; Mackay, K.; Friend, R. H.; Burn, P. L.; Holmes, A. B. *Nature* **1990**, *347*, 539−541.
(3) (a) Gustafsson, G.; Cao, Y.; Treacy, G. M.; Klavetter, F.; Colaneri, N.; Heeger, A. J. *Nature* **1992**, *357*, 477−479. (b) Gong, X.; Moses, D.; Heeger, A. J.; Liu, S.; Jen, A. K.-Y. *Appl. Phys. Lett.* **2003**, *83*, 183−185.
(4) (a) Baldo, M. A.; O'Brien, D. F.; You, Y.; Shoustikov, A.; Sibley, S.; Thompson, M. E.; Forrest, S. R. *Nature* **1998**, *395*, 151−154. (b) Baldo, M. A.; Lamansky, S.; Burrows, P. E.; Thompson, M. E.; Forrest, S. R. *Appl. Phys. Lett.* **1999**, *75*, 4−6. (c) Baldo, M. A.; Thompson, M. E.; Forrest, S. R. *Nature* **2000**, *403*, 750−753. (d) Tamayo, A. B.; Alleyne, B. D.; Djurovich, P. I.; Lamansky, S.; Tsyba, I.; Ho, N. N.; Bau, R.; Thompson, M. E. *J. Am. Chem. Soc.* **2003**, *125*, 7377−7387. (e) Sudhakar, M.; Djurovich, P. I.; Hogen-Esch, T. E.; Thompson, M. E. *J. Am. Chem. Soc.* **2003**, *125*, 7796−7797. (f) Kim, J. H.; Liu, M. S.; Jen, A. K.-Y.; Carlson, B.; Dalton, L. R.; Shu, C. F.; Dodda, R. *Appl. Phys. Lett.* **2003**, *83*, 776−778. (g) Carlson, B.; Phelan, G. D.; Kaminsky, W.; Dalton, L.; Jiang, X. Z.; Liu, S.; Jen, A. K.-Y. *J. Am. Chem. Soc.* **2002**, *124*, 14162−14172.
(5) (a) Handy, E. S.; Pal, A. J.; Rubner, M. F. *J. Am. Chem. Soc.* **1999**, *121*, 3525−3528. (b) Gao, F. G.; Bard, A. J. *J. Am. Chem. Soc.* **2000**, *122*, 7426−7427. (c) Buda, M.; Kalyuzhny, G.; Bard, A. J. *J. Am. Chem. Soc.* **2002**, *124*, 6090−6098.
(6) (a) Chen, F. C.; Yang, Y.; Thompson, M. E.; Kido, J. *Appl. Phys. Lett.* **2002**, *80*, 2308−2310. (b) He, G. F.; Chang, S. C.; Chen, F. C.; Li, Y. F.; Yang, Y. *Appl. Phys. Lett.* **2002**, *81*, 1509−1511. (c) Shao, Y.; Yang, Y. *Appl. Phys. Lett.* **2003**, *83*, 2453−2455. (d) Liu, J.; Shi, Y. J.; Yang, Y. *Appl. Phys. Lett.* **2001**, *79*, 578−580. (e) Shi, Y. J.; Liu, J.; Yang, Y. *J. Appl. Phys.* **2000**, *87*, 4254−4263. (f) Liu, J.; Guo, T. F.; Yang, Y. *J. Appl. Phys.* **2002**, *91*, 1595−1600.
(7) (a) Adachi, C.; Tsutsui, T.; Saito, S. *Appl. Phys. Lett.* **1989**, *55*, 1489−1491. (b) Pei, Q.; Yang, Y. *Adv. Mater.* **1995**, *7*, 559−561. (c) Kido, J.; Ohtani, C.; Hongawa, K.; Okuyama, K.; Nagai, K. *Jpn. J. Appl. Phys.* **1993**, *32*, 917−920. (d) Kido, J.; Kimura, M.; Nagai, K. *Science* **1995**, *267*, 1332−1334. (e) Hu, N. X.; Esteghamatian, M.; Xie, S.; Popovic, Z.; Hor, A. M.; Ong, B.; Wang, S. N. *Adv. Mater.* **1999**, *11*, 1460−1463. (f) Wang, J. F.; Jabbour, G. E.; Mash, E. A.; Anderson, J.; Zhang, Y. D.; Lee, P. A.; Armstrong, N. R.; Peyghambarian, N.; Kippelen, B. *Adv. Mater.* **1999**, *11*, 1266−1269. (g) Liu, S. F.; Wu, Q. G.; Schmider, H. L.; Aziz, H.; Hu, N. X.; Popovic, Z.; Wang, S. N. *J. Am. Chem. Soc.* **2000**, *122*, 3671−3678.
(8) (a) Hamada, Y. J.; Sano, T.; Fujita, M.; Fujii, T.; Nishio, Y.; Shibata, K. *Jpn. J. Appl. Phys.* **1993**, *32*, 514−515. (b) Hamada, Y. J.; Sano, T.; Shibata, K.; Kuroki, K. *Jpn. J. Appl. Phys.* **1995**, *34*, 824−826. (c) Hopkins, T. A.; Meerholz, K.; Shaheen, S.; Anderson, M. L.; Schmidt, A.; Kippelen, B.; Padias, A. B.; Hall, J. H. K.; Peyghambarian, N.; Armstrong, N. R. *Chem. Mater.* **1996**, *8*, 344−351. (d) Liu, S. F.; Seward, C.; Aziz, H.; Hu, N. X.; Popovic, Z.; Wang, S. N. *Organometallics* **2000**, *19*, 5709−5714. (e) Wu, Q. G.; Esteghamatian, M.; Hu, N. X.; Popovic, Z.; Enright, G.; Tao, Y.; D'Iorio, M.; Wang, S. N. *Chem. Mater.* **2000**, *12*, 79−83. (f) Leung, L. M.; Lo, W. Y.; So, S. K.; Lee, K. M.; Choi, W. K. *J. Am. Chem. Soc.* **2000**, *122*, 5640−5641. (g) Schmitz, C.; Schmidt, H. W.; Thelakkat, M. *Chem. Mater.* **2000**, *12*, 3012−3019. (h) Sapochak, L. S.; Padmaperuma, A.; Washton, N.; Endrino, F.; Schmett, G. T.; Marshall, J.; Fogarty, D.; Burrows, P. E.; Forrest, S. R. *J. Am. Chem. Soc.* **2001**, *123*, 6300−6307. (i) Sapochak, L. S.; Benincasa, F. E.; Schofield, R. S.; Baker, J. L.; Riccio, K. K. C.; Fogarty, D.; Kohlmann, H.; Ferris, K. F.; Burrows, P. E. *J. Am. Chem. Soc.* **2002**, *124*, 6119−6125. (j) Pohl, R.; Anzenbacher, P. J. *Organic Lett.* **2003**, *5*, 2769−2772.
(9) (a) Greenham, N. C.; Moratti, S. C.; Bradley, D. D. C.; Friend, R. H.; Holmes, A. B. *Nature* **1993**, *365*, 628. (b) Liu, Y. Q.; Yu, G.; Li, Q. L.; Zhu, D. B. *Synth. Met.* **2001**, *122*, 401−408.
(10) Noda, T.; Shirota, Y. *J. Am. Chem. Soc.* **1998**, *120*, 9714−9715.
(11) Garbuzov, D. Z.; Bulovi, V.; Burrows, P. E.; Forrest, S. R. *Chem. Phys. Lett.* **1996**, *249*, 433−437.
(12) Kepler, R. G.; Beeson, P. M.; Jacobs, S. J.; Anderson, R. A.; Sinclair, M. B.; Valencia, V. S.; Cahill, P. A. *Appl. Phys. Lett.* **1995**, *66*, 3618−3620.
(13) Deans, R.; Kim, J.; Machacek, M. R.; Swager, T. M. *J. Am. Chem. Soc.* **2000**, *122*, 8565−8566.
(14) (a) Lou, J.; Xie, Z.; Lam, J. W. Y.; Cheng, L.; Chen, H.; Qiu, C.; Kwok, H. S.; Zhan, X. W.; Liu, Y. Q.; Zhu, D. B.; Tang, B. Z. *Chem. Commun.* **2001**, 1740−1741. (b) Chen, J. W.; Law, C. C. W.; Lam, J. W. Y.; Dong, Y. P.; Lo, S. M. F.; Williams, I. D.; Zhu, D. B.; Tang, B. Z. *Chem. Mater.* **2003**, *15*, 1535−1546. (c) Chen, J. W.; Xie, Z. L.; Lam, J. W. Y.; Law, C. C. W.; Zhu, D. B.; Tang, B. Z. *Macromolecules* **2003**, *36*, 1108−1117. (d) Chen, J. W.; Peng, H.; Law, C. C. W.; Dong, Y. P.; Lam, J. W. Y.; Williams, I. D.; Tang, B. Z. *Macromolecules* **2003**, *36*, 4319−4327. (e) Lee, M. H.; Kim, D.; Lam, J. W. Y.; Tang, B. Z. *J. Korean Phys. Soc.* **2004**, *45*, 329−332.
(15) Sapochak, S. L.; Burrows, P. E.; Garbuzov, D.; Ho, D. M.; Forrest, S. R.; Thompson, M. E. *J. Phys. Chem.* **1996**, *100*, 17766−17771.
(16) Brinkmann, M.; Gadret, G.; Muccini, M.; Taliani, C.; Masciocchi, N.; Sironi, A. *J. Am. Chem. Soc.* **2000**, *122*, 5147−5157.
(17) Sano, K.; Kawata, Y.; Urano, T. I.; Mori, Y. *J. Mater. Chem.* **1992**, *2*, 767−768.
(18) Curioni, A.; Boero, M.; Andreoni, W. *Chem. Phys. Lett.* **1998**, *294*, 263−271.

of its optical behaviors.[16] Therefore, it is important to obtain the molecular crystal structures.

There has been current interest in the chemical, optical, and electronic properties of silole ring systems.[19] The silole ring is a new building unit of $\pi$-conjugated polymers with very small band gaps that exhibits intrinsic conductivity or semiconducting properties due to its unique electronic structure.[20] The high electron-accepting ability of the silole ring has been experimentally known. It has recently been theoretically demonstrated that the lowest unoccupied molecular orbital (LUMO) energy level of the silole ring is ascribed to the $\sigma^*-\pi^*$ conjugation between the $\sigma^*$ orbital of the exocyclic C−Si bonds on silicon and the $\pi^*$ orbital of the butadiene moiety in the ring.[21] These materials show excellent EL properties.[22] Murata and Tamao have reported that siloles having pyrrol-2-yl or bipyridin-6-yl substituents at the 2,5-positions, 2,5-bis-(2-pyridin)-1,1-dimethyl-3,4-diphenylsilole (PySPy) and 2,5-bis(6′-(2′,2″-bipyridyl))-1,1-dimethyl-3,4-diphenylsilole (PyPySPyPy), show excellent ET properties, as being applicable to the efficient ET materials in EL devices.[22b,e] PySPy could not be used as an emissive material because of its undesired formation of exciplexes (or CT complexes) with HT material TPD. The study showed that PyPySPyPy has a high mobility of $2 \times 10^{-4}$ cm$^2$/V·s that is over 2 orders of magnitude higher than that of $Alq_3$.[23] Recently, Murata has found that 1,2-bis(1-methyl-2,3,4,5-tetraphenylsilacyclopentadienyl)ethane (2PSP) gives a high $\phi_{PL}$ of 97 ± 3% in the vapor-deposited solid films.[22b] Devices using this silole derivative show a high external EL quantum efficiency ($\eta_{EL}$) of 4.8%. For silole-based organic LEDs, the best efficient devices have been fabricated with 1-methyl-1,2,3,4,5-pentaphenylsilole (MPPS) and 1,1,2,3,4,5-hexaphenylsilole (HPS) with an external $\eta_{EL}$ of 8% and 7%, respectively.[14c,22c] Therefore, 2,3,4,5-tetraarylsilole derivatives are a group of excellent emissive and ET material for LED application.

Recently, we have reported the AIE phenomenon for MPPS[14a] and demonstrated that the AIE phenomena are general characteristics for 1,1-disubstituted 2,3,4,5-tetraphenylsiloles.[14b] Our previous studies have mainly focused on photophysical properties and EL characteristics of these materials and the effects of solvent polarity and solution viscosity as well as temperature on their PL behaviors.[14,22c] The measured fluorescence lifetimes of MPPS[22c] and HPS[14e] indicate that the silole compounds are fluorescent materials. Organic LEDs using either MPPS or HPS show high external quantum efficiencies, which are close to the theoretical limit for a device using a fluorescent emitter.[14c,22c] To date, no information on the real origin of the excellent EL properties and the electronic structures is available. We anticipated that this work could offer us the opportunity to elucidate the origin of the unique EL characteristics of 2,3,4,5-tetraphenylsilole derivatives. In this work, we investigated in detail the crystal structures, thermogravimetric properties, PL, and charge carrier transport characteristics of 2,3,4,5-tetraphenylsilole derivatives having different substituents at the 1,1-positions, 1,1-dimethyl-2,3,4,5-tetraphenylsilole (DMTPS), MPPS, and HPS as well as carrying out related theoretical calculations. In contrast to our previous work, this contribution adds the following new insights: (1) The crystal structures of DMTPS and MPPS were obtained. Theoretical calculations and crystal structures indicate that the three siloles exhibit three-dimensional nonplanar structures in both solution and solid states. These molecular structures are helpful to reduce the formation of excimers and aggregation PL quenching in the solid states. (2) The electronic structures of the siloles were investigated using quantum chemical calculations and the effect of the substituents at the 1,1-positions on the $\pi$-electronic structures was discussed. (3) To reveal the microscopic origin of the peculiar luminescent behaviors, we studied the excited state decays of DMTPS. It is found that intramolecular rotation of the exocyclic phenyl groups has a large contribution to the nonradiative transition process, whose decay rate is 2−3 orders of magnitude larger than the radiative one. This can explain why DMTPS exhibits a faint emission in ethanol or chloroform, restricting the rotation of the peripheral side phenyl ring either by molecular aggregate, by molecular packing, or by lowering the temperature, which should induce the luminescence enhancement. (4) Fluorescence quantum yields and the carrier charge mobilties in thin films for the substituted siloles were measured. Experimental results suggest that high charge carrier mobilities and high PL efficiencies are the main origin of the excellent EL performances of MPPS and HPS.

## Experimental Section

**Thermal Analysis.** Thermogravimetric analysis (TGA) was carried out using a Perkin-Elmer thermogravimeter (model TGA7) under a dry nitrogen gas flow at a heating rate of 20 °C/min. Glass transition temperatures ($T_g$) and melting temperatures ($T_m$) were determined by differential scanning calorimetry (DSC) at a heating rate of 20 °C/min using a Perkin-Elmer differential scanning calorimeter (DSC7).

**X-ray Diffraction.** Single crystals of DMTPS, MPPS, and HPS were grown from methanol. Crystal data were obtained with graphine-monochromated Cu Kα radiation ($\lambda = 0.71073$ Å) on a Rigaku RAPID

(19) (a) Yamaguchi, S.; Jin, R. Z.; Tamao, K. *Organometallics* **1997**, *16*, 2230−2232. (b) Yamaguchi, S.; Jin, R. Z.; Tamao, K. *Organometallics* **1997**, *16*, 2486-2488. (c) Goldfuss, B.; Schleyer, P. V. R.; Hampel, F. *Organometallics* **1996**, *15*, 1755−1757. (d) Yamaguchi, S.; Jin, R. Z.; Ohno, S.; Tamao, K. *Organometallics* **1998**, *17*, 5133−5138. (e) Yamaguchi, S.; Tamao, K. *J. Organomet. Chem.* **2002**, *653*, 223−228. (f) Yamaguchi, S.; Xu, C. H.; Tamao, K. *J. Am. Chem. Soc.* **2003**, *125*, 13662−13663. (g) Yamaguchi, S.; Iimura, K.; Tamao, K. *Chem. Lett.* **1998**, 89−90. (h) Yamaguchi, S.; Endo, T.; Uchida, M.; Izumizawa, T.; Furukawa, K.; Tamao, K. *Chem. Lett.* **2001**, 98−99. (i) Kanno, K. I.; Ichinohe, M.; Kabuto, C.; Kira, M. *Chem. Lett.* **1998**, 99−100. (j) Adachi, A.; Ohshita, J.; Kunai, A.; Okita, K. *Jpn. J. Appl. Phys.* **1999**, *38*, 2148−2149. (k) Mäkinen, A. J.; Uchida, M.; Kafafi, Z. H. *Appl. Phys. Lett.* **2003**, *82*, 3889−3891. (l) Peng, H. J.; Liu, Z. T.; Chem. H. Y.; Ho, Y. L.; Tang, B. T.; Wong, M.; Huang, H. C. *J. Appl. Phys.* **2002**, *92*, 5735−5739. (m) Lee, J.; Liu, Q. D.; Motala, M.; Dane, J.; Gao, J.; Kang, Y.; Wang, S. N. *Chem. Mater*. **2004**, *16*, 1869−1877. (n) Lee, J.; Liu, Q. D.; Bai, D. R.; Kang, Y.; Tao, Y.; Wang, S. N. *Organometallics* **2004**, *23*, 6205−6213.

(20) (a) Liu, M. S.; Lou, J. D.; Jen, A. K.-Y. *Chem. Mater*. **2003**, *15*, 3496−3500. (b) Yamaguchi, S.; Jin, R. Z.; Itami, Y.; Goto, T.; Tamao, K. *J. Am. Chem. Soc.* **1999**, *121*, 10420−10421. (c) Yamaguchi, S.; Jin, R. Z.; Tamao, K. *J. Am. Chem. Soc.* **1999**, *121*, 2937−2938. (d) Ohshita, J.; Nodono, M.; Takata, A.; Kai, H.; Adachi, A.; Sakamaki, K.; Okita, K. *Macromol. Chem. Phys.* **2000**, *201*, 851−857. (e) Tamao, K.; Yamaguchi, S.; Ito, Y.; Matsuzaki, Y.; Yamabe, T.; Fukushima, M.; Mori, S. *Macromolecules* **1995**, *28*, 8668−8675. (f) Tamao, K.; Yamaguchi, S.; Shiro, M. *J. Am. Chem. Soc*. **1994**, *116*, 11715−11722.

(21) (a) Yamaguchi, S.; Itami, Y.; Tamao, K. *Organometallics* **1998**, *17*, 4910−4916. (b) Yamaguchi, S.; Jin, R. Z.; Tamao, K. *J. Organomet. Chem.* **1998**, *559*, 73−80. (c) Yamaguchi, S.; Tamao, K. *Bull. Chem. Soc. Jpn.* **1996**, *69*, 2327−2334.

(22) (a) Ohshita, J.; Nodono, M.; Kai, H.; Watanabe, T.; Kunai, A.; Komaguchi, K.; Shiotani, M.; Adachi, A.; Okichi, K.; Harima, Y.; Yamashita, K.; Ishikawa, M. *Organometallics* **1999**, *18*, 1453−1459. (b) Murata, H.; Kafafi, Z. H. *Appl. Phys. Lett.* **2002**, *80*, 189−191. (c) Chen, H. Y.; Lam, Y. W.; Luo, J. D.; Ho, Y. L.; Tang, B. Z.; Zhu, D. B.; Wong, M.; Kwok, H. S. *Appl. Phys. Lett.* **2002**, *81*, 574−576. (d) Uchida, M.; Izumizawa, T.; Nakano, T.; Yamaguchi, S.; Tamao, K.; Furukawa, K. *Chem. Mater*. **2001**, *13*, 2680−2683. (e) Tamao, K.; Uchida, M.; Izumizawa, T.; Furukawa, K.; Yamaguchi, S. *J. Am. Chem. Soc.* **1996**, *118*, 11974−11975. (f) Lee, J.; Liu, Q. D.; Motala, M.; Dane, J.; Gao, J.; Kang, Y.; Wang, S. N. *Chem. Mater*. **2004**, *16*, 1869−1877. (g) Palilis, L. C.; Mäkinen, A. J.; Uchida, M.; Kafafi, Z. H. *Appl. Phys. Lett.* **2003**, *82*, 2209−2211.

(23) Murata, H.; Malliaras, G. G.; Uchida, M.; Shen, Y.; Kafafi, Z. H. *Chem. Phys. Lett.* **2001**, *339*, 161−166.

IP imaging plate system. The structure was solved by direct method with SHELXL97 program and refined with full-matrix least-squares methods.

**Structure Computation Method.** The quantum chemical calculations for the siloles were carried out with DFT as implemented in the DMol3 package.[24,25] The basis set chosen was the double numerical plus d-functions (DND). The exchange-correlation was the Perdew−Wang functional (PWC). The core electrons for metals were treated by effective core potentials (ECP). Starting geometries for these optimizations were derived from the X-ray crystal structure.

**Transient Electroluminescence.** NPB and $Alq_3$ (purchased from Aldrich Chemical Co.) were purified by a train sublimation method. Organic LEDs were fabricated on 30 Ω/□ indium−tin oxide (ITO)-coated glass substrates using a conventional vacuum vapor deposition in a vacuum of $2 \times 10^{-4}$ Pa. The emitting area of the EL devices was 4 $mm^2$. The organic layers and electrodes were grown by means of conventional vacuum deposition. A quartz crystal oscillator placed near the substrate was used to measure the thickness of the thin films, which were calibrated ex situ using an Ambios Technology XP-2 surface profilometer. The absorption spectra of the silole thin films were studied using the quartz substrates. The absorption and PL spectra were recorded with a general TU-1201 UV−vis spectrophotometer and a Hitachi F-4500 fluorescence spectrophotometer, respectively. For the transient-EL experiment, an Agilent 8114A 100V/2 programmable pulse generator was used to apply rectangular voltage pulses to the devices. The repetition rate of the pulse was 1 kHz, and the pulse length was 10 $\mu$s. The time-dependent EL signals were detected by the 50 Ω input resistance of a digital oscilloscope (Agilent model 54815A, 500 MHz/2 G·s/s), together with a Hamamatsu photomultiplier (time resolution: 0.65 ns) located directly on top of the emitting devices.

## Theoretical Section

Under the displaced harmonic approximation, the Born−Oppenheimer nonradiative decay rate can be given in eq 1.[26]

$$W_{i-f}^{S_1-S_0} = \sum_l \frac{1}{\hbar^2}\left(\frac{\omega_l}{2\hbar}\left|R_l(fi)\right|^2\right)\mathrm{DWFCF} \tag{1}$$

$$\mathrm{DWFCF} = \sqrt{\frac{2\pi}{\sum_j{}' S_j\omega_j^2(2\bar{n}_j+1)}}\exp\left[-\frac{(\omega_{fi}+\omega_l+\sum_j{}' S_j\omega_j)^2}{2\sum_j{}' S_j\omega_j^2(2\bar{n}_j+1)}\right] \tag{2}$$

where initial state $i$ means the lowest singlet state $S_1$ (according to Kasha's rule, the molecular emission is from the lowest excited state), final state $f$ means the ground-state $S_0$, $R_l(fi) = -\hbar^2\langle\Phi_f|(\partial/\partial Q_l)|\Phi_i\rangle$, DWFCF means the density weighted Franck−Condon factor, $\omega_{fi}$ is the energy difference between the final state and the initial state, $S_j$ is the Huang−Rhys factor for the $j$th mode, and $\sum_j' S_j\omega_j$ is the sum of the relaxation energies for all modes except the promoting mode $l$, $\bar{n}_j$ is the thermally averaged numbers of phonon for $j$th mode in the Boltzman distribution. According to the linear coupling model,[27] the displacement in the normal mode coordinate $\Delta Q_j$ is obtained from the energy gradient of the excited state:

$$\Delta Q_j = \frac{G_j}{\omega_j^2} \tag{3}$$

$$G_j = \frac{\partial E^{\mathrm{exc}}}{\partial Q_j} \tag{4}$$

and the Huang−Rhys factor $S_j$ is obtained as

$$S_j = \frac{\omega_j \Delta Q_j^2}{2\hbar} \tag{5}$$

and the reorganization energy for $j$th mode is

$$\lambda_j = S_j\omega_j\hbar \tag{6}$$

It should be noted from eq 1 that for the decay rate to be large, both the electronic coupling prefactor and the DWFCF should be large. The electronic coupling term originates from the derivative of wave function with respect to the vibrational normal mode coordinate. For conjugated systems, for instance in linear polyene or polyacetylene, the normal mode from double-bond stretching has strong coupling with the electronic transition, which presents the dominant feature in the resonant Raman spectroscopy. It is noted that the larger the vibronic coupling, the larger the nuclear relaxation, and the larger the DWFCF (overlap). It is also noted that in DWFCF, the summation excludes the mode ($l$) which appears in the electronic coupling prefactor. Suppose that some vibrational modes contribute to the electronic coupling and some other modes contribute to DWFCF independently, then one can expect that the nonradiative decay will be fast, which would eventually quench the luminescence. We will see this is very important to understand the luminescent behavior for siloles.

The chemical structure of DMPTS, its normal coordinates, and vibration frequencies are obtained at the B3LYP/6-31g level. The excited-state energy gradient ($G_j$) is calculated numerically using the size of $dQ_j$ so that the Euclidean norm of the nuclear displacements is 0.01 Å. The energy of excited state is calculated at TDDFT B3LYP/6-31g level and performed by Gaussian 03 package program.[28]

## Results and Discussion

**Molecular Structure and X-ray Single-Crystal Diffraction.** The charge carrier mobility, $\Phi_{PL}$, volatility, film-forming ability, energy band, and environmental stability are key factors for

(24) (a) Delley, B. *J. Chem. Phys.* **1990**, *92*, 508−517. (b) Delley, B. *J. Chem. Phys.* **2000**, *113*, 7756−7764.
(25) Perdew, J. P.; Wang, Y. *Phys. Rev. B* **1992**, *45*, 13244−13249.
(26) (a) Lin, S. H. *J. Chem. Phys.* **1966**, *44*, 3768−3773. (b) Lin, S. H. *J. Chem. Phys.* **1966**, *44*, 3759−3767. (c) Lin, S. H.; Chang, C. H.; Liang, K. K.; Chang, R.; Zhang, J. M.; Yang, T. −S.; Hayashi, M.; Shiu, Y. J.; Hsu, F. C. *Adv. Chem. Phys.* **2002**, *121*, 1−88.
(27) (a) Macak, P.; Luo, Y.; Agren, H. *Chem. Phys. Lett.* **2000**, *330*, 447−456. (b) Sharp, T. E.; Rosenstock, M. *J. Chem. Phys.* **1964**, *41*, 3453−3463.
(28) Frisch, M. J.; Trucks, G. W.; Schlegel, H. B.; Scuseria, G. E.; Robb, M. A.; Cheeseman, J. R.; Montgomery, J. A.; Vreven, T., Jr.; Kudin, K. N.; Burant, J. C.; Millam, J. M.; Iyengar, S. S.; Tomasi, J.; Barone, V.; Mennucci, B.; Cossi, M.; Scalmani, G.; Rega, N.; Petersson, G. A.; Nakatsuji, H.; Hada, M.; Ehara, M.; Toyota, K.; Fukuda, R.; Hasegawa, J.; Ishida, M.; Nakajima, T.; Honda, Y.; Kitao, O.; Nakai, H.; Klene, M.; Li, X.; Knox, J. E.; Hratchian, H. P.; Cross, J. B.; Adamo, C.; Jaramillo, J.; Gomperts, R.; Stratmann, R. E.; Yazyev, O.; Austin, A. J.; Cammi, R.; Pomelli, C.; Ochterski, J. W.; Ayala, P. Y.; Morokuma, K.; Voth, G. A.; Salvador, P.; Dannenberg, J. J.; Zakrzewski, V. G.; Dapprich, S.; Daniels, A. D.; Strain, M. C.; Farkas, O.; Malick, D. K.; Rabuck, A. D.; Raghavachari, K.; Foresman, J. B.; Ortiz, J. V.; Cui, Q.; Baboul, A. G.; Clifford, S.; Cioslowski, J.; Stefanov, B. B.; Liu, G.; Liashenko, A.; Piskorz, P.; Komaromi, I.; Martin, R. L.; Fox, D. J.; Keith, T.; Al-Laham, M. A.; Peng, C. Y.; Nanayakkara, A.; Challacombe, M.; Gill, P. M. W.; Johnson, B.; Chen, W.; Wong, M. W.; Gonzalez, C.; Pople, J. A. Gaussian 03, Revision A.1, Gaussian, Inc., Pittsburgh, PA, 2003

***Table 1.*** Summary of Crystal Data for DMTPS, MPPS, and HPS, Including Data Collection and Refinement Details

| | DMTPS | MPPS | HPS[14b] |
|---|---|---|---|
| empirical formula | $C_{30}H_{26}Si$ | $C_{35}H_{28}Si$ | $C_{40}H_{30}Si$ |
| fw | 414.60 | 476.66 | 538.73 |
| crystal system | monoclinic | triclinic | triclinic |
| space group | $P2(1)/n$ | $P\bar{1}$ | $P\bar{1}$ |
| $a$, Å | 9.0912(18) | 10.1890(3) | 9.527(4) |
| $b$, Å | 18.649(4) | 11.2713(6) | 10.043(4) |
| $c$, Å | 28.255(6) | 11.9870(5) | 16.308(6) |
| $\alpha$, deg | 90 | 88.8270(4) | 77.150(7) |
| $\beta$, deg | 96.25(3) | 76.811(3) | 79.580(7) |
| $\gamma$, deg | 90 | 88.576(2) | 71.981(7) |
| $V$, Å$^3$ | 4761.9(16) | 1339.75(10) | 1435.9(9) |
| $Z$ | 8 | 2 | 2 |
| $F(000)$ | 1760 | 504 | 568 |
| $D$(calcd), mg/m$^3$ | 1.157 | 1.812 | 1.246 |
| $\mu$, mm$^{-1}$ | 0.113 | 0.109 | 0.110 |
| temp, K | 293(2) | 293(2) | 100(2) |
| $\lambda$, Å | 0.71073 | 0.71073 | 0.71070 |
| $2\theta$ range, deg | 1.31−27.48 | 2.94−27.48 | 1.31−25 |
| final $R$ indices [$I > 2\sigma(I)$] | $R_1 = 0.0745$ | $R_1 = 0.0535$ | $R_1 = 0.0639$ |
| | wR2 = 0.1908 | wR2 = 0.1093 | wR2 = 0.1048 |
| $R$ indices (all data) | $R_1 = 0.1466$ | $R_1 = 0.0962$ | $R_1 = 0.1002$ |
| | wR2 = 0.2144 | wR2 = 0.1213 | wR2 = 0.1150 |
| goodness-of-fit on $F^2$ | 1.027 | 0.92 | 0.952 |

determining EL properties of organic materials. These parameters are strongly coupled to molecular structure and bulk molecular-packing characteristics. Therefore, it is important to obtain the single crystal because X-ray diffraction on single crystals is the best method for providing their molecular structure and molecular packing. Furthermore, single crystals of 1,1-disubstituted 2,3,4,5-tetraphenylsiloles were prepared and their crystal structures were determined by X-ray crystallography to compare their structures and to discover how the molecular structures affect the optoelectronic properties of silole derivatives. Their crystal data are summarized in Table 1, and the selected bond lengths, bond angles, and torsion angles are listed in Table 2. The chemical and crystal structures of the siloles are shown in Figure 1. DMTPS crystallized in the monoclinic system space group $P2(1)/n$, while both MPPS and HPS crystallized in the triclinic system space group $P\bar{1}$. The crystal structure of DMTPS exhibits the two molecules in the asymmetric unit that mainly differ in the rotations of the phenyl groups with respect to the silole ring, presumably as a result of crystal packing forces. DMTPS crystals have structural parameters similar to that reported by Párkányi.[29] All three of the siloles contain an almost planar silole ring with torsion angles less than |6.5|°, while both siloles with thesame two substituents at silicon atoms (DMTPS and HPS) have better planarity than the one with two different substituents (MPPS). The crystal structures of all the siloles exhibit highly twisted conformations of phenyl groups at ring carbons in the silole skeleton. Rotation of the phenyl groups at ring carbons with respect to the silole's ring conforms to two-fold symmetry. The sense of the twist for all four phenyl groups is typically the same: either all clockwise or all anticlockwise in a particular molecule. In the crystal structures of DMTPS, a 1:1 mixture of clockwise (*cloc*-DMTPS) and anticlockwise (*ant*-DMTPS) forms is observed. Both conformers of DMTPS are highly twisted, while the degree of twist of the anticlockwise form is larger than that of the clockwise one. Only a clockwise form is obtained for both MPPS and HPS. The phenyl substituents at the ring carbons are twisted out of the plane of the silacyclopentadiene to varying extents, with great twists of −80.5° to −39.5° or 48.8 to 69.1° at the $C_{30}$, $C_{40}$, and $C_{50}$ positions for all siloles. HPS structure contains an unusual finding that one of the phenyl groups ($C_{10}$) is practically coplanar with the silole ring with the torsion angle $C_{16}-C_{11}-C_{10}-C_{20}$ being as small as 3.8(5)°. This better planarity can remarkably increase the conjugation degree. 1,1,2,3,4,5-Hexaphenylstannole has a molecular structure similar to that of HPS.[30] The dihedral angles between the mean plane of the central silole ring of DMTPS and the mean planes of its two benzene rings at the 2,5-positions are 47−62.4°. These are larger than those of 2,5-bis(*p*-methyoxyphenyl)silole, which has a highly coplanar arrangement of three rings, apparently due to the lack of the 3,4-substituents.[31] This noncoplanarity of DMTPS may arise from the steric repulsion between the neighboring phenyl groups at the ring carbons. Compared with DMTPS, MPPS has larger torsion angles at the 2,5-positions and smaller torsion angles at the 3,4-position, while the torsion angles at the 3,4-positions increase for HPS. Therefore, substitutes at silicon atom have a pronounced effect on the molecular structures and affect the twisting of phenyl groups at the ring carbons.

The endocyclic C−C (single) bond lengths of DMTPS are longer than those of the endocyclic C═C (double) bonds (mean C−C 1.521 vs C═C 1.353 Å), while the exocyclic Si−C bond lengths are shorter than those of the endocyclic Si−C bonds (1.846 vs 1.864 Å). Similar behavior is observed for the C−C bond lengths of MPPS and HPS. Compared with DMTPS, the Si−C bonds in HPS are somewhat stretched due to the steric effect of two bulky phenyl groups, whereas in MPPS this effect is lessened because of only one phenyl group at the 1,1-positions. The average endocyclic and the exocyclic C−Si−C bond angles of DMTPS are 92.68° and 109.7°, respectively, while those for MPPS decrease to 92.19° and 108.98° and those of HPS increase to 93.20° and 111.6°.

To achieve high efficiency in solid films and high luminance in LED devices, it is important to prevent self-quenching processes due to the formation of excimers in the solid state. The above results indicate that all of the three siloles have a three-dimensional nonplanar molecular structure and that the substituents at the 1,1-positions enhance the steric hindrance and considerablyaffect the degree of twist of the phenyl groups at the ring carbons. These nonplanar structures could reduce the intermolecular interaction and the possibility of excimer formation and thus increase PL efficiency of the solid films.

**Electronic Structure.** Some research groups have already reported theoretical analyses for silole and 1,1-dimethylsilole.[21a,32] Khabashesku et al. have recently analyzed the spectral data for silole in detail by ab initio calculations and pointed out that the longer absorption maxima of silole in comparison with those of cyclopentadiene are probably due to an increased cyclic hyperconjugation in the silole.[33] To clarify the role of the silicon

(29) Párkányi, L. *J. Organomet. Chem.* **1981**, *216*, 9−16.
(30) Ferman, J.; Kakareka, J. P.; Klooster, W. T.; Mullin, J. L.; Quattrucci, J.; Ricci, J. S.; Tracy, H. J.; Vining, W. J.; Wallace, S. *Inorg. Chem.* **1999**, *38*, 2464−2472.
(31) Katkevics, M.; Yamaguchi, S.; Toshimitsu, A.; Tamao, K. *Organometallics* **1998**, *17*, 5796−5800.
(32) Tamao, K.; Ohno, S.; Yamaguchi, S. *Chem. Commun*. **1996**, 1873−1874.
(33) Khabashesku, V. N.; Balaji, V.; Boganov, S. E.; Nefedov, O. M.; Michl, J.*J. Am. Chem. Soc*. **1994**, *116*, 320−329.

***Table 2.*** Experimental and Calculated Structural Parameters for the DMTPS, MPPS, and HPS Molecules

| structural parameter[a] | DMTPS | | MPPS | | HPS | | structural parameter[a] | DMTPS | | MPPS | | HPS | |
|---|---|---|---|---|---|---|---|---|---|---|---|---|---|
| | expel | calc | expel | calc | expel[14b] | calc | | expel | calc | expel | calc | expel[14b] | calc |
| Si−C10 | 1.858(3) | 1.866 | 1.867(2) | 1.868 | 1.874(3) | 1.865 | Si−C40−C30 | 108.2(2) | 107.40 | 108.1(1) | 107.57 | 107.1(2) | 106.88 |
| | 1.872(3) | 1.869 | | | | | | 107.8(2) | 107.45 | | | | |
| Si−C40 | 1.860(3) | 1.868 | 1.869(2) | 1.868 | 1.862(3) | 1.865 | C10−C20−C30 | 115.5(3) | 116.30 | 115.6(2) | 116.53 | 117.0(3) | 116.67 |
| | 1.864(3) | 1.868 | | | | | | 116.2(3) | 116.33 | | | | |
| C10−C20 | 1.358(4) | 1.366 | 1.361(2) | 1.367 | 1.357(4) | 1.370 | C20−C30−C40 | 115.5(3) | 116.37 | 115.6(2) | 116.14 | 116.0(3) | 116.05 |
| | 1.355(4) | 1.367 | | | | | | 115.7(3) | 116.37 | | | | |
| C20−C30 | 1.528(4) | 1.483 | 1.512(2) | 1.485 | 1.501(4) | 1.482 | C40−Si−C10 | 92.79(15) | 92.39 | 92.19(8) | 92.44 | 93.20(13) | 93.02 |
| | 1.515(4) | 1.483 | | | | | | 92.57(14) | 92.37 | | | | |
| C30−C40 | 1.349 (4) | 1.367 | 1.363(2) | 1.365 | 1.358(4) | 1.366 | C5−Si−C6 | 109.6 (2) | 110.45 | 108.98(9)[e] | 110.02 | 111.6(3)[f] | 111.05 |
| | 1.351(4) | 1.366 | | | | | | 109.8(2) | 110.75 | | | | |
| Si−C5 | 1.843(3) | 1.863 | 1.868(2)[c] | 1.866 | 1.874(3)[c] | 1.867 | C16−C11−C10−C20 | −43.6(5) | −35.16 | −53.4 (3) | −30.93 | 3.8(5) | −16.95 |
| | 1.844(3) | 1.862 | | | | | | 34.8(5) | 31.78 | | | | |
| Si−C6 | 1.842(4) | 1.865 | 1.854(2) | 1.866 | 1.864(3)[d] | 1.862 | C26−C21−C20−C30 | −57.2(4) | −51.06 | −51.3 (2) | −52.51 | −80.5(4) | −56.23 |
| | 1.854(4) | 1.863 | | | | | | 69.1(4) | 50.93 | | | | |
| C10−C11 | 1.489(4) | 1.452 | 1.481(2) | 1.452 | 1.480(3) | 1.450 | C36−C31−C30−C20 | −57.3(4) | −52.32 | −53.9 (3) | −51.36 | −61.6(1) | −53.87 |
| | 1.481(4) | 1.452 | | | | | | 66.4(4) | 52.54 | | | | |
| C20−C21 | 1.478(4) | 1.467 | 1.490(2) | 1.467 | 1.488(3) | 1.467 | C46−C41−C40−C30 | −39.5(5) | −30.72 | −46.2 (3) | −32.96 | −39.5(5) | −35.19 |
| | 1.486(4) | 1.467 | | | | | | 48.8(5) | 32.88 | | | | |
| C30−C31 | 1.482(4) | 1.467 | 1.488(2) | 1.466 | 1.494(3) | 1.467 | Si−C10−C20−C30 | 3.4(3) | 1.93 | 4.7 (2) | 1.71 | −0.6(3) | −3.76 |
| | 1.478 (4) | 1.467 | | | | | | 1.2(3) | −1.58 | | | | |
| C40−C41 | 1.488(4) | 1.451 | 1.476(2) | 1.451 | 1.479(3) | 1.451 | C10−C20−C30−C40 | −2.4(4)) | −1.74 | −6.5 (2) | −2.40 | −3.2(4) | −0.70 |
| | 1.483(4) | 1.451 | | | | | | 3.5(4) | 2.58 | | | | |
| Sl−C10−C20 | 107.9(2) | 107.51 | 108.3(1) | 107.28 | 106.3(2) | 106.60 | | | | | | | |
| | 107.3(2) | 107.43 | | | | | | | | | | | |

[a] Bond and torsion angles are reported in degrees, while bond lengths are in angstroms. [c] Si−C51. [d] Si−C61. [e] C51−Si−C6. [f] C51−Si−C61.

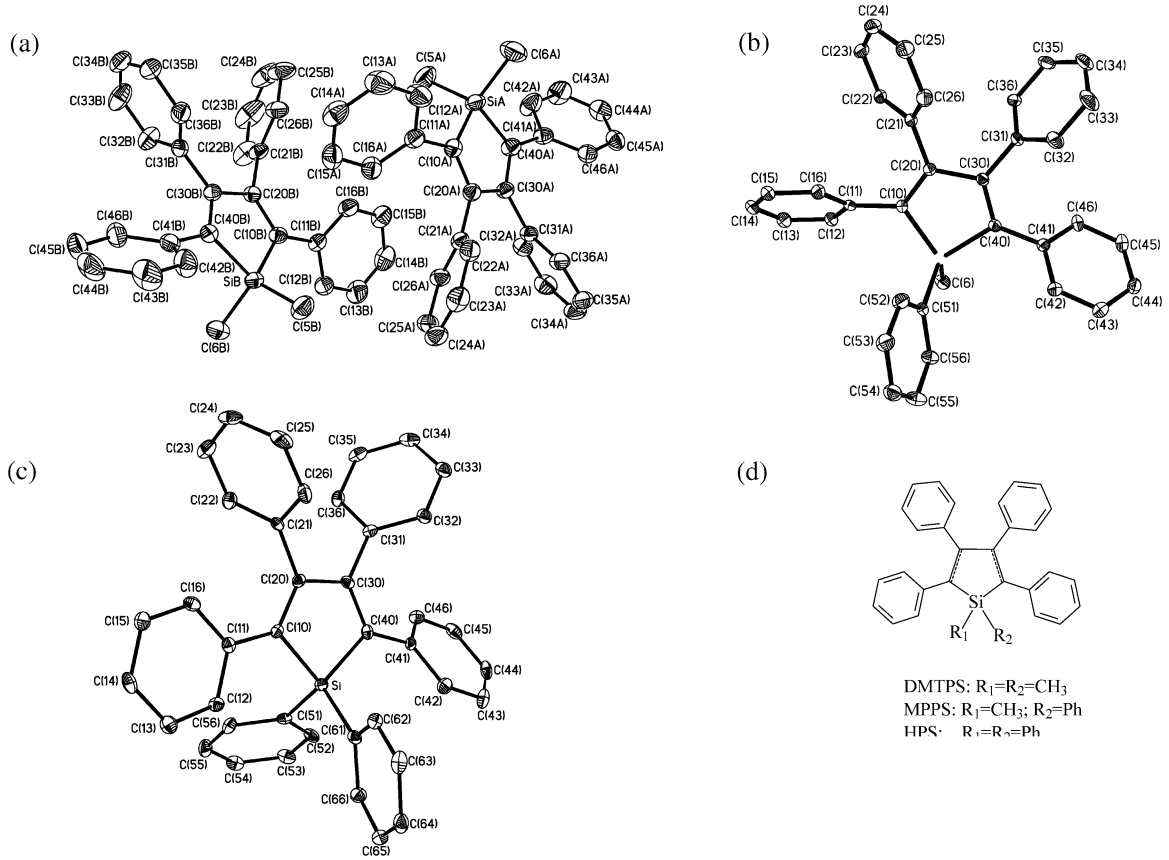


***Figure 1.*** Crystal structures of the DMTPS (a), MPPS (b), and HPS (c), and their chemical structures (d).

atom in the electronic structure of the silole ring, Tamao et al. have compared the electronic structure of the silole with that of cyclopentadiene based on HF/6-31G* calculations.[34] The silole has a lower highest occupied molecular orbital (HOMO) by about 0.4 eV and a much lower-lying LUMO by about ∼1.3 eV than those of cyclopentadiene. The PM3 calculations indicate that the silole ring has a considerably low-lying LUMO, arising from $\sigma^*-\pi^*$ conjugation between a $\pi$-symmetry $\sigma^*$ orbital of the exocyclic $\sigma$ bonds on silicon and a $\pi^*$ orbital of the butadiene skeleton. The $\sigma^*-\pi^*$ conjugation and the low-lying LUMO would thus be the origin of the unusual optical properties of silole derivatives.[21c] To describe the substituent effect on the electronic structures of the silole ring by the groups on the ring silicon atom, namely the 1,1-disubstituents, theoretical calculations on their electronic structures were carried out. The calculated values for the pertinent geometrical parameters are comparable to the experimental ones determined in the X-ray

(34) Yamaguchi, S.; Tamao, K. *Tetrahedron Lett.* **1996**, *37*, 2983−2986.

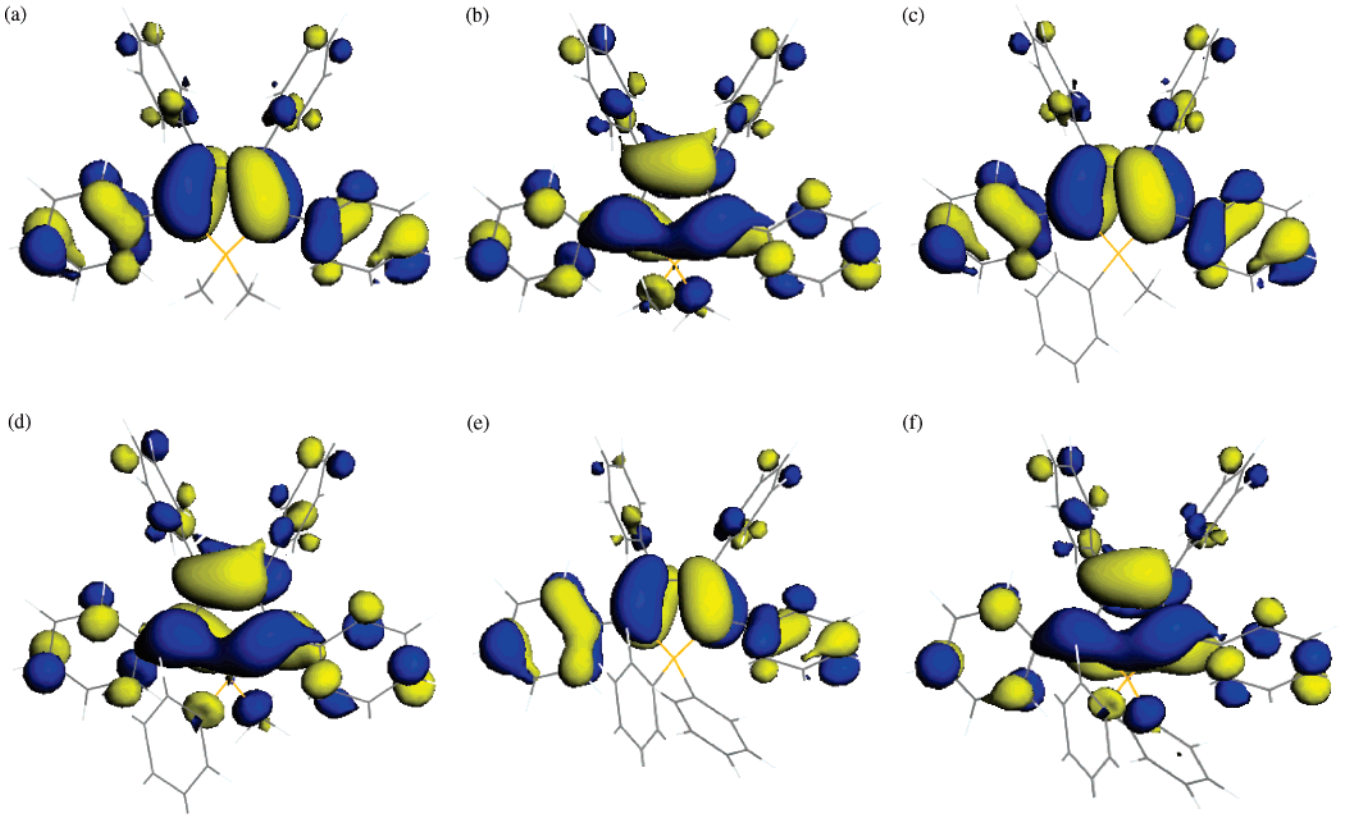


***Figure 2.*** Molecular orbital amplitude plots of the HOMO (a) and LUMO (b) of the DMTPS molecule, HOMO (c) and LUMO (d) of the MPPS molecule, and HOMO (e) and LUMO (f) of the HPS molecule.

structure of the three siloles (see Table 2). In our calculations for the isolated molecules of DMTPS, the clockwise and anticlockwise optimized forms turn out to be equal in energy and dipole moment. It is reasonable to expect that the two isomers could easily be transformed to each other and coexist in the amorphous thin film state. Both the clockwise and anticlockwise optimized forms of DMTPS have almost the same bond lengths, bond angles (within 0.40°), and torsion angles (within 3.4°), but with opposite torsion directions. The optimized bond lengths and bond angles of DMTPS show good agreement with the experimental determination, but torsion parameters reveal a large variation. These result in a more open, less spherically compressed structure, which can be attributed to the absence of packing effects in the calculation. Therefore, we could expect that the optimized structures are closely similar to that in a dilute solution at low temperature. The optimized structures of DMTPS are less twisted than the corresponding crystal structures. This indicates that the optimized structures have a better coplanar and larger conjugation degree compared with those of the crystal structures. Similarly, both the optimized structures of MPPS and HPS exhibit smaller torsion degrees than their crystal structures. The optimized bond lengths and bond angles for the three siloles are also identical. The optimized structure of each silole exhibits almost identical torsion angles at the 3- and 4-positions; simultaneously, the torsion angles at the 2,5-positions are very close, not counting the *cloc*-DMTPS and HPS. Therefore, the substituents at the 1,1-positions have a pronounced effect on the torsion of phenyl groups at the 2,5-positions but do not affect those at the 3,4-positions. The successive substitution of a methyl group by the phenyl group at the 1,1-position decreases the torsion degree of the phenyl

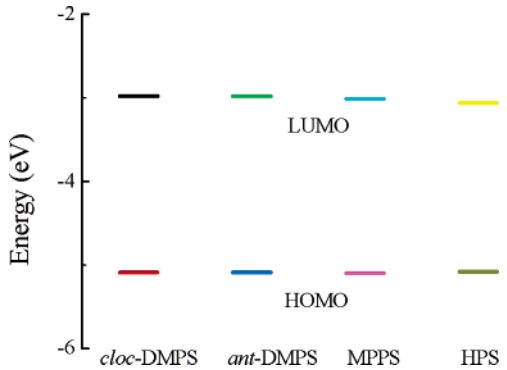


***Figure 3.*** Diagram of the calculated orbital energy levels for the DMTPS, MPPS, and HPS molecules.

group at the 2-position, whereas that at the 5-position is increased. The HOMOs and LUMOs for all three siloles display qualitatively similar surfaces as shown in Figure 2. The filled $\pi$ orbitals (or HOMOs) and the unfilled orbitals (or LUMOs) are mainly dominated by orbitals originating from the silole ring and two phenyl groups at the 2,5-positions in all cases, while the LUMOs have significant orbital density at two exocyclic $\sigma$ bonds on the ring silicon, implying that the $\sigma^*-\pi^*$ conjugation plays an important role. The relative energy levels for the 1,1-disubstituted 2,3,4,5-tetraphenylsiloles are depicted in Figure 3. Both the HOMO and LUMO energy levels for the three siloles have close data, which do not depend on the number of phenyl groups at silicon atoms. Previous theoretical calculations have shown that the 1,1-substituents largely affect the HOMO and LUMO energy levels of the silole ring mainly due to their inductive effects.[21b]

***Table 3.*** Calculated Variation of Bond Lengths (Å) in the Cation and the Anion for the DMTPS, MPPS, and HPS Molecules, Relative to the Neutral Molecules

| | DMTPS | | MPPS | | HPS | |
|---|---|---|---|---|---|---|
| structural parameter | cation | anion | cation | anion | cation | anion |
| Si−C10 | 0.009 | −0.012 | 0.013 | 0.009 | 0.013 | −0.021 |
| | 0.011 | −0.015 | | | | |
| C10−C20 | 0.032 | 0.039 | 0.029 | 0.038 | 0.029 | 0.039 |
| | 0.030 | 0.039 | | | | |
| C20−C30 | −0.032 | −0.037 | −0.035 | −0.038 | −0.034 | −0.037 |
| | −0.034 | −0.037 | | | | |
| C30−C40 | 0.031 | 0.037 | 0.030 | 0.036 | 0.029 | 0.035 |
| | 0.030 | 0.038 | | | | |
| Si−C40 | 0.009 | −0.014 | 0.010 | −0.015 | 0.014 | −0.013 |
| | 0.012 | −0.014 | | | | |
| C10−C11 | −0.020 | −0.016 | −0.022 | −0.015 | −0.023 | −0.013 |
| | −0.021 | −0.015 | | | | |
| C20−C21 | −0.011 | −0.006 | −0.008 | −0.007 | −0.008 | −0.007 |
| | −0.008 | −0.006 | | | | |
| C30−C31 | −0.010 | −0.006 | −0.008 | −0.005 | −0.007 | −0.005 |
| | −0.008 | −0.006 | | | | |
| C40−C41 | −0.021 | −0.014 | −0.020 | −0.013 | −0.018 | −0.011 |
| | −0.020 | −0.014 | | | | |
| Si−C5 | −0.007 | 0.016 | −0.015[a] | 0.018[a] | −0.012[a] | −0.012[a] |
| | −0.008 | 0.017 | | | | |
| Si−C6 | −0.008 | 0.014 | −0.012 | −0.015 | −0.014[b] | 0.018[b] |
| | −0.008 | 0.016 | | | | |

[a] Si−C51. [b] Si−C61.

***Table 4.*** Calculated Variation of Bond Angles (deg) in the Cation and the Anion for the DMTPS, MPPS, and HPS Molecules, Relative to the Neutral Molecules

| | DMTPS | | MPPS | | HPS | |
|---|---|---|---|---|---|---|
| structural parameter | cation | anion | cation | anion | cation | anion |
| Si−C10−C20 | 1.783 | −0.490 | 1.391 | −0.288 | 1.628 | −0.210 |
| | 1.465 | −0.384 | | | | |
| C10−C20−C30 | −0.719 | 0.044 | −0.521 | −0.253 | −0.926 | −0.487 |
| | −0.463 | 0.010 | | | | |
| C20−C30−C40 | −0.705 | 0.046 | −0.425 | 0.254 | −0.508 | 0.302 |
| | −0.512 | 0.006 | | | | |
| C30−C40−Si | 1.771 | −0.398 | 1.444 | −0.536 | 1.536 | −0.689 |
| | 1.474 | −0.392 | | | | |
| C40−Si−C10 | −2.112 | 0.815 | −1.979 | 0.778 | −2.477 | 0.773 |
| | −1.979 | 0.794 | | | | |
| C6−Si−C5 | 1.441 | −4.107 | 2.332[a] | −4.169[a] | 1.959[b] | −4.099[b] |
| | 2.334 | −4.258 | | | | |

[a] C51−Si−C6. [b] C51−Si−C61.

**Cation and Anion Properties.** The operation of organic LEDs involves the injection of both electrons and holes from opposite electrodes, their transport in the bulk materials, recombination to form excitons, and the radiative decay of the excitons giving rise to electroluminescence. Therefore, information about the change of molecular structure versus the injection of one charge is important to understand PL and EL properties of the three siloles. To evaluate the effects of charge injection on the molecular conformations, we calculated structural and electronic properties of both the anion and the cation. For this purpose, geometry optimization was carried out on both molecular ions of the three siloles (i.e., the neutral molecule in the presence of an extra electron and that of an extra hole, respectively). Tables 3, 4, and 5 list the variation in the bond lengths, bond angles, and torsion angles. The cations or the anions for both the clockwise and anticlockwise forms of DMTPS have nearly same bond lengths (within 0.01 Å), bond angles (within 1.2°), and torsion angles at the 3,4-positions (within 1.9°), but with opposite torsion directions. Compared

***Table 5.*** Calculated Variation of Torsion Angle (deg) in the Cation and the Anion for the DMTPS, MPPS, and HPS Molecules, Relative to the Neutral Molecules

| | DMTPS | | MPPS | | HPS | |
|---|---|---|---|---|---|---|
| structural parameter | cation | anion | cation | anion | cation | anion |
| C16−C11−C10−C20 | 2.464 | 14.644 | 10.729 | 12.367 | −0.582 | 2.303 |
| | −5.885 | −10.868 | | | | |
| C26−C21−C20−C30 | 1.383 | 2.058 | −1.346 | 3.763 | 5.615 | 8.803 |
| | 0.582 | −2.236 | | | | |
| C36−C31−C30−C20 | 1.406 | 2.982 | −0.933 | 1.143 | −2.789 | 1.023 |
| | 0.343 | −3.451 | | | | |
| C42−C41−C40−C30 | 1.880 | 10.054 | 6.759 | 8.982 | 8.523 | 8.967 |
| | −8.010 | −11.714 | | | | |
| C10−C20−C30−C40 | 2.578 | 0.333 | 5.755 | 2.1 | 4.381 | 1.314 |
| | −5.377 | −1.216 | | | | |
| Si−C10−C20−C30 | −0.672 | −0.856 | −5.662 | −3.471 | −5.674 | −2.067 |
| | 4.121 | 0.675 | | | | |

to those of anticlockwise form, the optimized structures for both the cation and the anion of the clockwise form show similar structural changes relative to those of the neutral DMTPS molecule. Both the anion and cation exhibit a smaller torsion degree than that in the neutral DMTPS molecule, indicating that both the anion and cation have a better coplanarity and a larger conjugation degree than the neutral molecule. One surprising result is obtained for DMTPS and MPPS, wherein the carrier injection considerably decreases the torsion degree of the phenyl groups at the 2,5-positions, which leads to a dramatic increase of the coplanarity of the silole and the two phenyl rings at the 2,5-positions. For HPS, we obtain a different result such that the carrier injection leads to a remarkable decrease in the torsion degree at the 3,5-positions. The cation of MPPS exhibits a close twist at the 3- and 4-positions to the neutral molecule, while the cation and the anion have almost same torsion degree at the 3-position. When either a hole or an electron is injected, the endocyclic C−C single bond distances increase, and the endocyclic C−C double bonds lengths decrease, whereas a close variation in degree of twist was obtained for the anion or cation. Electron injection decreases the endocyclic Si−C distances with the exception of the endocyclic Si−C10 length of MPPS and extends the exocyclic Si−C lengths except for the exocyclic Si−C6 length of MPPS and the exocyclic Si−C51 length of HPS. In contrast to the anions, the endocyclic Si−C bond lengths increase and the exocyclic Si−C bond distances decrease for the cation. Adding an electron has more pronounced effects on the change of the Si−C bond length than adding a hole. Change of the bond angles is mainly localized on the C−Si−C bond angles. The anions have a larger endocyclic C−Si−C bond angle and a smaller exocyclic C−Si−C bond angle than those of the neutral molecules. An opposite behavior is found in the cations. On the basis of the structural relaxation for both the cation and the anion discussed above, we should expect that the silole molecules will exhibit a relatively high coplanarity between the central silole ring and the two phenyl rings at the 2,5-positions versus the injection of one charge, especially negative.

Table 6 shows the calculated values of the ionization potentials (IPs) and the electron affinities (EAs) for the DMTPS, MPPS, and HPS molecules. The clockwise and anticlockwise forms of DMTPS reveal identical IPs and EAs. Substituents at the silicon atom have somewhat of an effect on the IPs and Eas. The successive substitution of the methyl group by the phenyl group at the 1,1-positions leads to a decrease of the IPs

***Table 6.*** Calculated Ionization Potentials, and Electron Affinities for the DMTPS, MPPS, and HPS Molecules (in eV)

| silole | IP(v)[a] | IP(a) | EA(v) | EA(a) |
|---|---|---|---|---|
| DMTPS | 6.81 | 6.70 | −1.26 | −1.43 |
| | 6.81 | 6.67 | −1.26 | −1.43 |
| MPPS | 6.77 | 6.63 | −1.35 | −1.54 |
| HPS | 6.72 | 6.58 | −1.44 | −1.60 |

[a] (v) and (a) indicate vertical and adiabatic values, respectively.

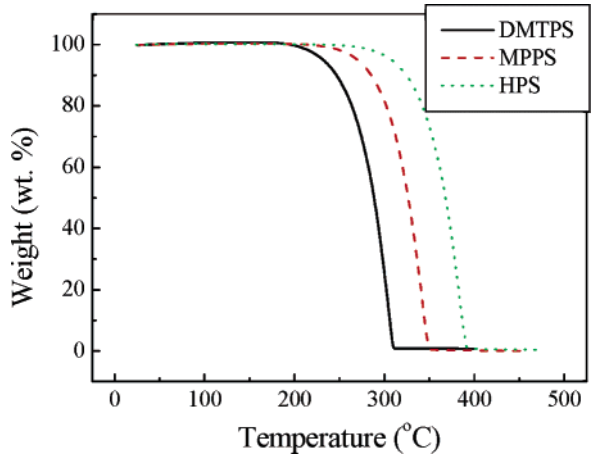


***Figure 4.*** TGA curves of the DMTPS, MPPS, and HPS.

and EAs. Both vertical IPs and EAs are larger than the corresponding adiabatic values for the three siloles. A different result was observed for both the molecular isomers of $Alq_3$.[35] Addition of one hole or one electron to the $Alq_3$ molecule promotes a relatively small structural relaxation. The vertical IP and the EA for $Alq_3$ have almost identical values as those of the adiabatic ones. These were obtained as results for $Zn(BTZ)_2$ and $[Zn(BTZ)_2]_2$, which are similar to $Alq_3$.[36]

**Thermal Stability.** The thermal properties of the three siloles were evaluated by TGA and DSC experiments. The TGA scans for three siloles are shown in Figure 4. All siloles in our study exhibit different weight-loss behavior, where the magnitude of the weight loss depends on the numbers of phenyl rings on 1,1-positions and the decomposition temperature increases with an increase of the numbers of phenyl rings (onset: 271.6 °C for DMTPS, 308.7 °C for MPPS, and 350.9 °C for HPS). We observed double endothermic transitions ($T_m$) at 160 and 183.8 °C with only a 2% weight loss prior to decomposition of the MDPS at 271 °C. Upon phenyl substitution of DMTPS, $T_m$ increases in the order of MPPS < DMTPS < HPS. In addition, two endothermic transitions similar to those for DMTPS are observed for MPPS; however, an endothermic transition at 190 °C is observed only for HPS. The glassy state of DMTPS is difficult to form by cooling crystalline material at a rate of 20 °C/min immediately following the melting transition in both the first and second heating cycles. The second heating cycles of MPPS and HPS reveal a glass transition ($T_g$) at 54 and 65 °C, respectively. The above results suggest that the difference of thermal properties is considerable for 1-phenylated and 1,1-diphnylated derivatives compared to those of the 1-unphenylated analogues.

**Photoluminescence Properties.** The PL properties of the DMTPS, MPPS, and HPS in polar solvents have been studied.[14b] We measured their PL characteristics in a nonpolar solvent, cyclohexane, to remove the effect of the solvent polarity and obtain the real PL performances. The UV−vis absorption and PL data for the three siloles are summarized in Table 7. In the absorption spectra, all siloles exhibit absorption maxima ($\lambda_{max}$) at 350−380 nm in both solution and thin films. DMTPS has ~5−7 nm shorter $\lambda_{max}$ than those of the other two siloles, which have almost the same absorption maxima. Only a single emission peak was observed for all three siloles in polar solvents.[14b,30] However, we observed a different result where the three siloles in a nonpolar solvent, cyclohexane, show a main emission peak to the accompaniment of a shoulder peak. This phenomenon is very obvious at low temperature, where the PL spectra are narrowed. The emission maxima as well as absorption peaks significantly depend on the number of phenyl rings at the 1,1-positions. The successive replacement of the methyl group by the phenyl ring at the 1,1-positions gradually leads to a red-shift of PL spectra. The UV−visible absorption and PL spectra of the 2,5-diaryl-3,4-diphenylsiloles were systematically evaluated,[37] and it is found that the photophysical properties significantly depend on the nature of the 2,5-aryl groups.

In comparison with those in solution, the absorption and emission spectra of all the DMTPS, MPPS, and HPS films are red-shift only to a small extent. This implies that the intermolecular interactions in solution for these molecules are rather weak in the solid states. It has previously been observed that 2,3,4,5-tetraarylsiloles containing pyridyl groups essentially have similar absorption and PL spectra in both solid state and solution.[22d] Most of "normal" luminescent materials in thin films exhibit wider emission spectra than those in solution due to stronger intermolecular interactions in the solid state. An opposite trend is, however, observed for the three siloles, whose emission spectra in the film states are obviously narrower than those in solution. This result is very consistent with the twisted conformation in both solution and solid state proved by quantum chemical calculations and X-ray analysis. In solution, the intramolecular rotation of peripheral phenyl rings around the axes of the single bonds linked to the central silole ring may widen the emission spectra. In the film states, the stacking forces involved in the molecular packing may restrict the intramolecular rotations, thus narrowing the emission spectra. This narrow emission in film states could be useful for improvement of the EL chromaticity.

1,1-Dimethyl-2,5-bisphenylsilole (DMBPS) has a high quantum yield of 29% in chloroform due to the highly coplanar arrangement of three rings.[31] The introduction of phenyl groups at the 3,4-positions significantly reduces the quantum yield because of the twisted conformation.[31] Yamaguchi et al. found that 1,1-dimethyl-2,5-diaryl-3,4-diphenylsiloles have very low PL efficiencies (0.044−0.25%) in chloroform, except for 1,1-dimethyl-2,5-distyryl-3,4-diphenylsilole.[37] These compounds have propeller-like arrangements of the four aryl rings at the 2,3,4,5-positions and nonplanar structures similar to those of our siloles. We also observe a similar result where the three siloles are poorly luminescent in cyclohexane with their luminescent efficiencies being 0.22% for DMTPS, 0.13% for

(35) Curioni, A.; Boero, M.; Andreoni, W. *Chem. Phys. Lett.* **1998**, *294*, 263−271.
(36) Yu, G.; Yin, S. W.; Liu, Y. Q.; Shuai, Z. G.; Zhu, D. B. *J. Am. Chem. Soc.* **2003**, *125*, 14816−14824.
(37) Yamaguchi, S.; Endo, T.; Uchida, M.; Izumizawa, T.; Furukawa, K.; Tamao, K. *Chem. Eur. J.* **2000**, *6*, 1683−1692.

**Table 7.** UV−Vis Absorption and PL Data for the DMTPS, MPPS, and HPS

| compd | $\lambda^{abs}_{max}$ (nm)[a] | $\lambda^{abs}_{max}$ (nm)[b] | $\lambda^{f}_{max}$ (nm)[a] | $\lambda^{f}_{max}$ (nm)[b] | $\Phi_f$ [a] (%) | $\Phi_f$ [b] (%) | fwhm (nm)[a,c] | fwhm (nm)[b,c] |
|---|---|---|---|---|---|---|---|---|
| DMTPS | 358 | 364 | 470, 488 | 460 | 0.22 | 76 | 100.6 | 73 |
| MPPS | 363 | 371 | 471, 494 | 494 | 0.13 | 85 | 105.6 | 95.2 |
| HPS | 363 | 373 | 474, 497 | 498 | 0.30 | 78 | 108 | 94 |

[a] In cyclohexane solution. [b] In thin films. [c] Full width at half-maximum of PL spectra.

MPPS, and 0.30% for HPS. When the temperature is decreased from 298 to 77 K, the PL intensities of the three siloles increase 59−84 times due to the restriction of the intramolecular rotation at low temperature.[14b] Thus, we can assume that the three siloles have rather low fluorescent quantum yields in the dilute solution mainly due to the highly twisted conformation of phenyl groups at the ring carbons of the silole skeleton and to the intramolecular rotation of the phenyl rings.

The PL quantum yields of the three silole films were estimated relative to that of an $Alq_3$ thin film. It has been reported that $\Phi_{Alq3}$ in solid state is 32%.[11] The three siloles exhibit high luminescent efficiencies, 76% for DMTPS, 85% for MPPS, and 78% for HPS. Interestingly, 2PSP, containing two 2,3,4,5-tetraphenylsilole rings, shows unusually high $\Phi_{PL}$ of 97 ± 3% in solid organic films.[22b,g] This compound can have a three-dimensional nonplanar molecular structure similar to those of the siloles studied in this contribution. This nonplanar structure could reduce the intermolecular interactions and prevent the self-quenching induced by the formation of excimers. Therefore, the 2,3,4,5-tetraphenylsiloles exhibit high PL quantum yields in the solid films because of the unique propeller-like arrangements of the four aryl rings at 2,3,4,5-positions.

**Excited State Decays.** To better understand the unique photophysical properties of 1,1-disubstituted 2,3,4,5-tetraphenylsiloles, we calculated the excited state decays of DMTPS. $\Phi_{PL}$ can be expressed as: $\Phi_{PL} = k_r/(k_r + k_{nr} + k_{ISC})$, where $k_r$ and $k_{nr}$ are the radiative and nonradiative decay rate, respectively, and $k_{ISC}$ is the intersystem crossing rate from the singlet state to the triplet one. The radiative decay can be evaluated through the Einstein spontaneous emission relationship which can be cast into a simple working formula $k_r = f \times E_{if}^2/1.499$, where $f$ and $E_{if}$ are the oscillator strength for the excited state and the excited-state energy, respectively. $E_{if}$ and $f$ can be evaluated by quantum chemical calculations. We carried out TD-DFT calculation using a B3LYP/6-31g basis set. The radiative decay rates are calculated to be $1.20 \times 10^8$ and $4.04 \times 10^8$ $s^{-1}$ for the theoretical molecular geometry and crystal structure, respectively. This result indicates that the molecule in the crystal has a slightly larger radiative decay rate than in gas phase. However, we believe that this small difference is not enough to explain the marked difference between luminescent properties in organic solvents and solid states. This suggests that nonradiative decay or the intersystem crossing must influence luminescent characteristics in a major way. The spin−orbit (SO) coupling constant between the lowest singlet excited state ($S_1$) and the lowest triplet state ($T_1$) is calculated at CAS (4,4)/6-31g level within the quantum chemical package Gamess to be 1.6 $cm^{-1}$, which is too small as compared with the radiative decay rate. This implies that the nonradiative decay must be a major way for the excited state decays.

The vibration normal modes are calculated by using the linear coupling model in eqs 3−6. The Huang−Rhys factors and the normal mode displacements between ground state ($S_0$) and the excited state $S_1$ for DMPTS are listed in Table 8. The excited-state energy gradient ($G_j$) is calculated numerically using the size of $dQ_j$ so that the Euclidean norm of the nuclear displacements is 0.01 Å, which is sufficiently small to guarantee the accuracy of the numerical derivation. It is most interesting to point out that the contributions from the low-frequency modes (<100 $cm^{-1}$) to the Huang−Rhys factors are very remarkable. These modes are related to the intramolecular rotations of the peripheral aromatic rings linked to the central silole core. We also note that the 130th mode (1573.4 $cm^{-1}$) is due to the C═C double bond stretching in the five-member silacycle, and its reorganization energy is 1584 $cm^{-1}$.

**Table 8.** Huang−Rhys Factors for the Most Displaced Vibration Modes of Compound DMTPS

| mode | $\omega_i$($cm^{-1}$) | $\Delta Q_i$(a.u.) | $S_i$ |
|---|---|---|---|
| 1 | 24.5 | −756.3 | 31.84 |
| 3 | 35.4 | 624.7 | 31.47 |
| 5 | 51.1 | 404.9 | 19.08 |
| 7 | 58.7 | 139.0 | 2.59 |
| 10 | 70.6 | −241.2 | 9.36 |
| 11 | 97.7 | −111.9 | 2.79 |
| 130 | 1573.4 | 16.8 | 1.01 |

The double bond stretching along the conjugation backbone is responsible for the electronic coupling prefactor in eq 1, while the low-frequency side-ring twisting motion contributes mostly to the Franck−Condon factor where the double bond stretching is excluded. Therefore, intramolecular rotations of the peripheral phenyl rings linked to the central silole core are favorable to the Born−Oppenheimer nonradiative decay. By forming clusters or aggregates, by molecular packing, or by adding sticky solvent, the side-ring twisting motions are restricted, the Franck−Condon factor is reduced, and then, the nonradiative decay is slowed, leading to the luminescent enhancements. It has been found that the coupling is mainly due to this mode, and it has been calculated to be around 1800 $cm^{-1}$ for several conjugated molecules.[38] In this way, the nonadiabatic radiationless transition rate at room temperature is calculated to be $1.8 \times 10^{11}$ $s^{-1}$, which is much faster than the radiative decay. This indicates that the excited state is mainly dissipated through nonradiative channels in the compound DMTPS, resulting in the faint emission in organic solvents. We further calculated the temperature dependence of the nonradiative decay process (see Supporting Information). It is found that the nonradiative transition rate is remarkably reduced with decreasing temperature. Therefore, the restricting intramolecular rotations of the peripheral phenyl rings by either molecular packing or lowering the temperature would induce the luminescence enhancement, in good agreement with the experimental results.[14]

**Charge Transport Properties and Transient Electroluminescence.** To achieve high EL efficiency in organic LEDs, balanced charge injections from both electrodes and comparable

(38) (a) Orlandi, G.; Zerbetto, F.; Zgierski, M. Z. *Chem. Rev.* **1991**, *91*, 867−891. (b) Troisi, A.; Orlandi, G. *J. Chem. Phys.* **2003**, *118*, 5356−5363.

mobilities of electrons and holes within the organic layer are necessarily required. The former can be achieved either by using metals with low work functions as cathodes or by adjusting the HOMO/LUMO levels of the organic layer. Unfortunately, it is very difficult for the latter to be achieved because of the intrinsic carrier transport properties of organic semiconducting materials, i.e., mobilities of holes are usually orders of magnitude higher than those of electrons. Therefore, it is of great importance to understand the fundamental mechanism of charge carrier mobility in organic materials and to investigate the effect of either substituent or morphology on the charge carrier mobility of organic materials. By changing organic film morphology from amorphous, polycrystalline to single crystal, both the hole and electron mobilities are drastically increased. Recently, Lee et al. have compared the charge transport characteristics of three EL polymers poly{2-(9′,9′-dihexylfluorenyl)-1,4-phenylene vinylene}s (DHF−PPV).[39] The introduction of an electron-donating or an electron-withdrawing group to the fluorene unit in DHF−PPV results in a decrease in the hole mobility. The effect of substitution on the charge carrier mobility in siloles has not been reported, although many attempts have been made to quantify this effect on hole mobility in triarylamines.[40] To compare the ET properties of the three siloles, we fabricated devices with the following structures ITO/NPB(30 nm)/silole-(60 nm)/$Alq_3$(5 nm)/LiF(1 nm)/Al, where silole is either DMTPS (device A), or MPPS (device B), or HPS (device C). The EL spectrum of each device is similar to the PL spectrum of the corresponding silole used. This result indicates that the light emission originates from the intrinsic emission of the siloles.

Figure 5 shows the voltage dependence of the transient EL of ITO/NPB/silole/$Alq_3$/LiF/Al devices upon application of a rectangular voltage pulse. With increasing voltage, a decrease in delay time ($t_d$) and a steeper rise in the EL were observed. Figure 6 shows the electron mobilities of the siloles plotted as a function of the square root of a bias field. It can be seen that the electron mobility in MPPS as well as in HPS shows an increase with the square root of the electric field. This kind of field-dependent mobility is typical in organic EL materials. The electron mobility of the HPS film lies in the range of 2.7−3.4 $\times 10^{-6}$ $cm^2/V\cdot s$ in the electric fields ranging from $8.3 \times 10^5$ to $1.8 \times 10^6$ V/cm. The electron mobility of $Alq_3$ measured by using the transient EL technique is $2.3 \times 10^{-6}$ $cm^2/V\cdot s$ at $1.2 \times 10^6$ V/cm.[41] HPS exhibits a higher mobility of $3.0 \times 10^{-6}$ $cm^2/V\cdot s$ than $Alq_3$, while MPPS shows a value of $2.1 \times 10^{-6}$ $cm^2/V\cdot s$ comparable to that of $Alq_3$ at the same electric field. For the DMTPS, no charge carrier mobility was determined due to its weak EL property and the poor film-forming ability. Tamao et al.[22e] compared the ET performance of PySPy with that of $Alq_3$. It was found that the device consisting of PySPy as the ET material and $Alq_3$ as the emissive material exhibits nearly 3 times higher $I-V$ efficiency than that obtained with a device using only $Alq_3$ as both the ET material and the emissive material. A recent study has shown that PyPySPyPy exhibits an excellent ET property, which is attributed to a large electron affinity originating from a $\sigma^*-\pi^*$ conjugation and a high aromaticity of anionic species.[23] At any given electric field, the electron mobility of the HPS film is about 1.4−1.5 times higher than that of MPPS film, that is, a better ET property is attained within the HPS layer. This certainly suggests that the $\pi$-electron-rich and bulky phenyl group in HPS facilitates ET when compared to the $\pi$-electron-poor and small methyl group in MPPS. To the best of our knowledge, the effect of substitution on charge carrier mobilities of siloles has not been reported before.

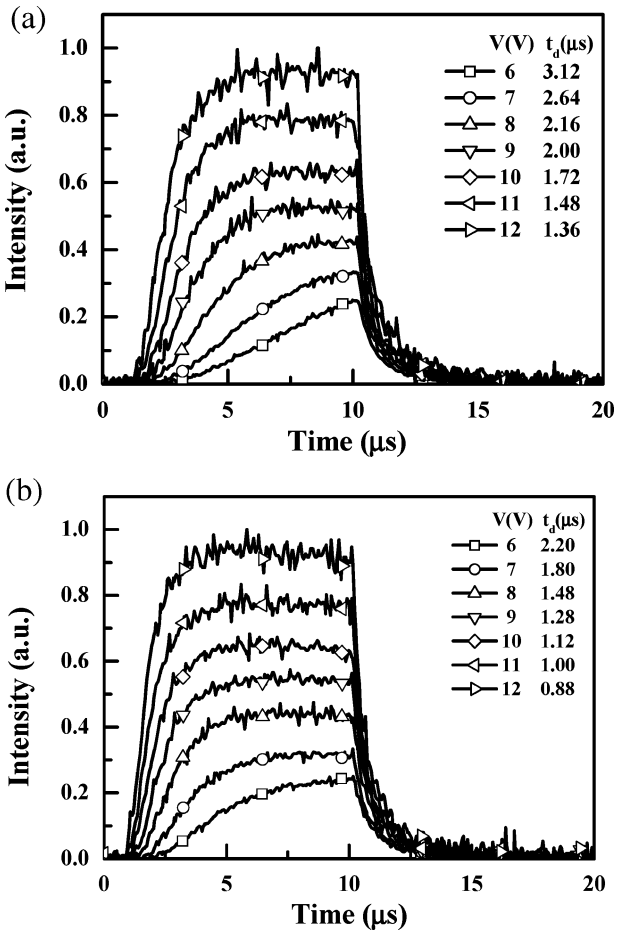


***Figure 5.*** Voltage dependence of the transient EL of ITO/NPB/MPPS/$Alq_3$/LiF/Al (a) and ITO/NPB/HPS/$Alq_3$/LiF/Al (b) devices upon application of a rectangular voltage pulse.

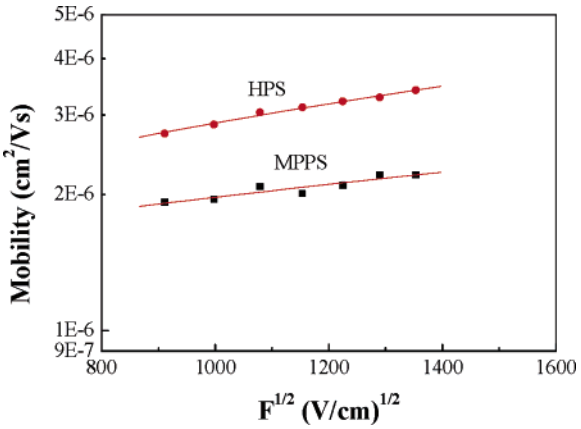


***Figure 6.*** Electron mobilities of the siloles plotted as a function of the square root of a bias field.

(39) Lee, S. H.; Yasuda, K.; Tsutsui, T. *J. Appl. Phys.* **2004**, *95*, 3825−3827.
(40) (a) Bender, T. P.; Graham, J. F.; Duff, J. M. *Chem. Mater.* **2001**, *13*, 4105−4111. (b) Maldonado, J. L.; Bishop, M.; Hernandez, C. F.; Caron, P.; Domercq, B.; Zhang, Y. D.; Barlow, S.; Thayumanavan, S.; Malagoli, M.; Bredas, J. L.; Marder, S. R.; Kippelen, B. *Chem. Mater.* **2003**, *15*, 994−999.
(41) Ma, D. G.; Wang, G.; Hu, Y. F.; Zhang, Y. G.; Wang, L. X.; Jing, X. B.; Wang, F. S. *Appl. Phys. Lett.* **2003**, *82*, 1296−1298.

One efficient approach for increasing charge carrier mobilities is to improve morphological order in organic solid films by precise control of the substrate temperature. This method is not fit for the devices with multilayered structures because heating of the substrate may induce morphological changes in the underlying layers and diffusion of organic layer between the interfaces. Therefore, achieving high electron mobility in amorphous solid films is one of the most important challenges in the development of ET materials. It has been attempted to adjust the hole mobilities of triarylamines by introduction of the substituents, which results in a decrease in the hole mobilities.[40a] The best mobility value was obtained in the unsubstituted triarylamines. Maldonado et al. obtained a similar result wherein substituted TPD derivatives exhibited lower mobilities than the regular TPD parent.[40b] Therefore, adjusting the molecular structure of organic materials and introduction of the substituents into the organic molecule would be useful for tuning the charge carrier mobility of organic materials.

In principle, the efficiency of EL depends on the quantities of injected carriers (holes and electrons) as well as high $\Phi_{PL}$ of the emissive materials in solid films. A balanced injection of holes and electrons, a balanced carrier transport, and a high PL efficiency are required to realize an efficient EL. It has recently been experimentally demonstrated that MPPS and HPS exhibit EL efficiencies ($\eta_{EL}$) of 8 and 7%, respectively.[14c,22c] As described above, both MPPS and HPS thin films show excellent charge carrier transport properties and excellent PL characteristics. Therefore, we consider that the excellent EL performances of MPPS and HPS are mainly attributed to the high electron mobility and high PL efficiency in the solid films. MPPS exhibits a slower electron mobility and a higher PL efficiency in thin film than HPS. The improvement of the performance of the devices based on MPPS as compared with that based on HPS should be attributable primarily from its higher PL quantum efficiency. Some 2,3,4,5-tetraarylsilole derivatives exhibit unique EL properties with high electron mobility or high PL quantum efficiency.[22b,d,23] These materials have molecular structures similar to those of the siloles investigated by us.[32] The propeller-like arrangements of the four aryl rings and the planar silole ring would guarantee a three-dimensional nonplanar molecular structure and a suitable conjugation degree that could reduce the intermolecular interactions and the possibility of the formation of excimers, and increase the PL efficiency at the solid state. Thus, the above research work could be useful to understand the unique optoelectronic properties of 2,3,4,5-tetraarylsilole derivatives and to design novel, excellent EL materials with both high PL quantum efficiency and high charge carrier mobility.

## Conclusions

Experimental and theoretical studies of the molecular and electronic structures of 1,1-disubstited 2,3,4,5-tetraphenylsiloles are presented. In the crystal structures of DMTPS, a 1:1 mixture of clockwise and anticlockwise forms is observed. Only is clockwise form obtained for both MPPS and HPS. The crystal structures of the siloles exhibit highly twisted conformations of phenyl groups at the ring carbons of the silole skeleton and contain an almost planar silole ring. The degree of twist of the phenyl groups depends on the number of phenyl rings at the 1,1-positions.

Quantum chemical calculations combined with Born−Oppenheimer nonradiative decay calculations show that the combinations of double bond stretching and side-ring twisting enhance the radiationless process, which suppresses radiative channels. Aggregation formation or molecular packing can restrict the ring twisting, thus slowing the nonradiative decay process, and then the luminescence is recovered.

The theoretical analysis and crystal structures show the existence of the nonplanar structures in both solution and solid state for the three siloles. The electronic structures of the three siloles are investigated using quantum chemical calculations. The charge carrier mobilities in MPPS and HPS were measured using transient electroluminescence. The mobility of MPPS is comparable to that of $Alq_3$, while the mobility of HPS is about 1.4−1.5 times higher than that of MPPS film. It is found that the thin films of three siloles exhibit high PL efficiencies.

**Acknowledgment.** We thank Drs. H. W. Ma and Y. Li for X-ray analysis. This work was supported by the Major State Basic Research Development Program, the National Natural Science Foundation of China, and the Chinese Academy of Sciences.

**Supporting Information Available:** X-ray crystallographic data in CIF format and calculated temperature dependence of the nonradiative decays rate. This material is available free of charge via the Internet at http://pubs.acs.org.

JA044628B